Water Air Soil Pollut (2014) 225:2096
DOI 10.1007/s11270-014-2096-5

Rapid Removal of Heavy Metal Cations by Novel Nanocomposite Hydrogels Based on Wheat Bran and Clinoptilolite: Kinetics, Thermodynamics, and Isotherms

Aboulfazl Barati · Elham Abdollahi Moghadam · Taghi Miri · Mahdieh Asgari

Received: 6 February 2014 / Accepted: 24 July 2014 / Published online: 7 August 2014

Abstract Novel nanocomposite hydrogels based on wheat bran-g-poly(methacrylic acid) and nano-sized clinoptilolite have been successfully utilized for the removal of Pb(II), Cu(II), Cd(II), and Ni(II) cations from their aqueous solution. The experimental results were investigated using Freundlich, Langmuir, Temkin, and Dubinin–Radushkevich isotherm models. The pseudo-first-order, pseudo-second-order and interparticle diffusion kinetic models were studied in order to analyze the kinetic data. The kinetic data indicated that the rate of cation adsorption on nanocomposite hydrogels was fast that more than 80 % of the equilibrium adsorption capacity occurs within 15 min. The maximum monolayer adsorption capacity of the nanocomposite hydrogel, as obtained from the Langmuir adsorption isotherm, was found to be 166.7, 243.9, 175.4, and 166.6 mg g^{-1} for Pb(II), Cu(II), Cd(II), and Ni(II), respectively. Thermodynamic parameters such as free energy (ΔG^0), enthalpy (ΔH^0), and entropy (ΔS^0) change were determined; the sorption process was found to be endothermic. The results of five times sequential adsorption–desorption cycle showed high adsorption efficiency and a good degree of desorption.

Keywords Fast removal · Nanocomposite · Hydrogel · Clinoptilolite · Wheat bran · Kinetic · Heavy metals

A. Barati (✉) · E. A. Moghadam · T. Miri · M. Asgari
Chemical Engineering Department, Faculty of Engineering, Arak University, Arak 38156-8-8349, Iran
e-mail: a-barati@araku.ac.ir

1 Introduction

Metals are unique among pollutants that can be extremely harmful to the soil, water, and human beings (Lee et al. 2009; Lee and Kim 2010; Max Roundhill 2004). Regardless of how metals are used in consumer products or industrial processes, the improper disposal of these chemicals can cause serious environmental problems (Tavakoli and Yoshida 2005; Yoshizaki and Tomida 2000). An increase in the intake of Cu(II) may increase the risk of serious diseases such as vomiting, hypotension, melena, gastrointestinal distress, and kidney failure (Kayaalt et al. 2010) while high Ni(II) intake can lead to nasopharynx, lung, and dermatological diseases and birth defects (Xu et al. 2011). On the other hand, Pb(II) and Cd(II) have no immediate effect on the human body but have cause several serious problems such as kidney damage, disruption of the nervous system, and chronic metabolic disorders (Bannon et al. 2009; Matz and Krone 2007). Therefore, it is essential to do further research on finding new methods for controlling these heavy metals in the water and/or waste water to minimize or even eliminate their environmental impact (Giannopoulou and Panias 2007).

Filtration (Molinari et al. 2008), electrochemical treatment (Akbal and Camc 2011; Gupta et al. 2007a), solvent extraction (Ramachandra Reddy and Neela Priya 2005), oxidation–reduction (Gupta et al. 2007b; Gupta et al. 2012; Karthikeyan et al. 2012), reverse osmosis (Qdais and Moussa 2004), membrane separation (Pośpiech and Walkowiak 2007), and adsorption (Gupta et al. 2006a; Gupta et al. 2006b; Ghaee et al.

2012; Gupta et al. 2010; Mittal et al. 2010a; Mittal et al. 2005; Saleh and Gupta 2012) are the main traditional treatment methods that can be used for metal laden effluents. Because of the high operation cost and low metal ion retention capacity of these methods, using low-cost adsorbents is an effective and more economical method to adsorb and remove the variety of contaminants (Gupta et al. 2006a; Gupta et al. 2007c; Gupta et al. 2011a; Gupta et al. 2011b; Gupta and Rastogi 2009; Uğuzdoğan et al. 2010).

Recently, the adsorption process with strong affinity and high loading capacity for targeted metal ions has got much attention, which leads to modification of hydrogels (Demirbilek and Özdemir Dinç 2012). Hydrogels are loosely cross-linked hydrophilic polymers that can absorb and retain water up to hundred times their weight (Barati et al. 2010).

Natural hydrogels based on polysaccharides such as starch, flour, and agricultural waste grafted on biodegradable polymers are more favored than the synthetic polymers in making absorbent. This is simply because of the several advantages of natural hydrogels such as being cheaper, biodegradable, and leaving low polymer residues in the ecosystem (Gupta et al. 2007d; Gupta et al. 2009; Gupta et al. 2011c; Jain et al. 2003; Jain et al. 2004; Mittal et al. 2008; Mittal et al. 2010b; Reis et al. 2008; Salam et al. 2010).

Some attempts have been made to modify/optimize the properties of hydrogels; for example, the incorporation of nanoparticles or microparticles of inorganic materials such as clinoptilolite (Hua et al. 2010), kaolin (Pourjavadi et al. 2008), mica (Limparyoon et al. 2011), bentonite (Shirsath et al. 2011), laponite (Li et al. 2009), attapulgite (Zhang et al. 2007a), copper (Pourbeyram and Mohammadi 2014), silver (Jovanović et al. 2011), and zeolites (Bhardwaj et al. 2012) into polymer networks has been recently investigated.

Although many works have focused on the improvement of the swelling ability (Zhang et al. 2009), gel strength (Xu et al. 2010), and mechanical and thermal stability (Huang et al. 2007) of composite hydrogel, only few works have focused on improving the adsorption and removal capacity of heavy metals by the composite hydrogels (Hou et al. 2012; Nüket Tirtom et al. 2012; Yan et al. 2012).

Therefore, on the basis of our previous work on the preparation and ability to remove Pb(II) and Cd(II) by poly(acrylamide-co-acrylic acid) modified with porous materials (e.g., zeolites) (Zendehdel et al. 2011) and removal of Cu(II) and Ni(II) by poly(methacrylamide-co-acrylic acid)/montmorillonite nanocomposite (NC) (Barati et al. 2013), the adsorption capacity of low-cost novel NC hydrogel based on wheat bran and clinoptilolite for heavy metal cations (Pb(II), Cd(II), Cu(II), and Ni(II)) was studied in this paper. Fourier transform infrared (FTIR) spectroscopy, scanning electron microscopy (SEM), X-ray diffraction (XRD), and thermogravimetric analysis (TGA) techniques were used to characterize as-prepared NC hydrogels. The effect of clinoptilolite and wheat bran content (weight percent), contact time with solution, pH, temperature, and initial concentration of the cation solutions (C_0) were investigated. In addition, the regeneration and reusability of the adsorbents were also evaluated.

2 Materials and Methods

2.1 Chemicals

Methacrylic acid (MAAc, Merck, Germany) was distilled under reduced pressure before use. Lead nitrate ($Pb(NO_3)_2$), cadmium nitrate ($Cd(NO_3)_2$), copper nitrate ($Cu(NO_3)_2$), and nickel nitrate ($Ni(NO_3)_2$) were supplied by Merck, Germany. Sodium hydroxide (NaOH) and *N*,*N*′-methylene bisacrylamide (Bis) were supplied by Merck, Germany. Ammonium persulfate (APS, analytical grade, Merck, Germany) was recrystallized. The zeolite used was a clinoptilolite (CLI) obtained from Pars Kansar Shargh Co, Khorasan, Iran. The material was 73 % CLI, 13 % feldspar, and 13 % quartz, with traces of clay minerals. The particle size of zeolite aggregates ranges between 200 and 400 μm. Nano-sized CLI (with the average particle size of 70 nm measured by a particle size analyzer (Microtrac, Bluewave, USA)) was performed by wet milling of CLI aggregates using a planetary ball mill (PM 100, Retsch, Germany) for 2 to 4 h. Zirconium oxide balls of 3 mm were utilized for milling. Wheat bran (WB, Molaee flour mill industries, Iran) was used in experiments after treatment. Other agents were all of analytical grade, and all solutions were prepared with distilled water.

2.2 Preparation of Wheat Bran-g-Poly(Methacrylic Acid)/Clinoptilolite Nanocomposite Hydrogel

A series of NC hydrogels with different amounts of WB, neutralized MAAc, and CLI were prepared using the

one-step method via in situ intercalated polymerization. Typically 10 g of WB powder and 120 mL of distilled water were put in a 250-mL four necked flask equipped with a stirrer, a condenser, a thermometer, and a nitrogen line. The slurry was heated to 95 °C for 30 min under nitrogen line. In a 50-mL beaker, 14 mL of MAAc was partially neutralized by 21 mL NaOH (50 wt% aqueous solution) in an ice bath and then mixed with 5 mg of Bis as cross-linking agent. Different amounts of CLI (1 to 10 wt% based on MAAc) were loaded into the monomer solution and dispersed by an ultrasonic (Hielscher, UP400S, Germany) for 1 h at room temperature. The obtained suspension in the beaker was slowly added to flask when the temperature reached 60–65 °C. The obtained suspension was mixed by a 300-rpm mechanical stirrer for 30 min. After removal of oxygen, the initiator APS (60 mg) was then added, and temperature was raised to 80 °C and kept for 3 h to complete the polymerization reaction. Then, the resulting product was taken out of the flask, washed several times with hydro ethanol solution and soaked in distilled water, and dried at 70 °C to a constant weight. The dried product was milled and screened. All samples used had a particle size in the range of 60–80 mesh.

2.3 Characterization

FTIR spectra of WB, wheat bran-g-poly(methacrylic acid) (WB-g-PMAAc), and WB-g-PMAAc/CLI NC hydrogel were recorded (PerkinElmer, Spectrum 100) using KBr pellets. XRD patterns were obtained using a Philips X'Pert PRO Alpha-1 diffractometer (Cu K radiation, λ=1.54056 Å, 40 kV, 40 mA) scanning from 2 to 25° at 2°/min. The morphology of the samples was observed on a SEM instrument (XL30, Philips Company, Netherlands), using secondary electron imaging, after sputter coating with gold under vacuum. TGA was performed using a PerkinElmer (TGA 4000) Thermal Analyzer in air at a heating rate of 15 °C/min in the temperature range of 25–600 °C.

2.4 Adsorption Experiment

Adsorption experiments were performed in batch equilibrium mode. A 100 mL of metal solution with known concentration containing 0.1 g of synthetic NC hydrogel in a 250-mL Erlenmeyer flask was agitated in an orbital shaker (THZ-98A) at 300 rpm in a temperature-controlled water bath (298 K) for a given contact time (5 to 180 min). The pH values of initial solutions were adjusted with 0.1 mol L^{-1} HCl or NaOH solutions by using a pH meter (Metrohm-744). The solution is filtered using a Whatman #40 filter paper. The filtrate was analyzed using inductively coupled plasma optical emission spectrometry (ICP-OES) PerkinElmer Optima™ series using wavelength 220.35, 226.5, 231.6, and 324.75 nm for Pb(II), Cd(II), Ni(II), and Cu(II), respectively (Futalan et al. 2011; Lara et al. 2001).

Ten different concentrations of metal ions between 25 and 700 mg L^{-1} were chosen as the initial concentration of cations solutions for isotherm studies. The effects of pH were studied in the pH range of 2–11 at an initial concentration of 25 or 100 mg L^{-1} for cations and contact time of 60 min. The adsorption capacity was calculated according to the following equation:

$$q_e = \frac{(C_0 - C_e)V}{m} \quad (1)$$

where q_e is the adsorption capacity, the amount of solute sorbed at equilibrium (mg g^{-1}), C_0 and C_e are the initial and final or equilibrium cation concentration (mg L^{-1}), m (g) is the mass of adsorbent used, and V is the volume of cation solution (mL). The calibration of the instrument was performed every time and prior to the sample analysis. The instrument calibrated with the standard solution of fluoride purchased from Merck, Germany. All the experiments were done in triplicate, and average values are reported.

2.5 Desorption and Regeneration

Desorption experiments were done in batch equilibrium mode by dispersing used (loaded) adsorbent (adsorbent dose in adsorption experiment=100 mg/100 mL; temperature=298 K; contact time=60 min; pH=6.8; CLI content=3 wt%) into two different volumes (10 and 20 mL) of 1 mol L^{-1} HCl solution at eluent (10 and 20 mL) and agitating at 298 K for 90 min in the orbital shaker. The desorbed cations were obtained and measured (using ICP-OES PerkinElmer Optima™ series). Then, the sample was treated three times in 0.1 mol L^{-1} NaOH solution at 300–310 K for 2 h under stirring. Subsequently sample was washed, filtered, and dried to obtain a regenerated NC hydrogel.

3 Results and Discussion

3.1 Fourier Transform Infrared Spectral Analysis

The FTIR spectra of (a) WB, (b) WB-g-PMAAc hydrogel, and (c) WB-g-PMAAc/CLI NC hydrogel containing 3 wt% CLI are shown in Fig. 1. As shown in Fig. 1a, the peak at 3,394 cm^{-1} is related with the hydrogen-bonded –OH stretching vibration. The absorption at 2,918 cm^{-1} arises from the –C=C–H stretching. The absorption at 1,734 cm^{-1} is caused by carbonyl group in carboxyl and esters. The peaks at 1,635 and 1,433 cm^{-1} are attributed to aromatic skeletal vibration and >N–H stretching, respectively. Furthermore, one can see the bands at 779, 470, and 397 cm^{-1} related to –C–H deforming, Si–O–Ca bending, and Fe–O, respectively (Dupont and Guillon 2003).

The absorption bands in Fig. 1b at 1,666 and 1,602 cm^{-1} are ascribed to –COOH stretching and COO^{-} asymmetric stretching, respectively. It confirms that a part of MAAc was neutralized by KOH solution. Some peaks corresponding to WB cannot be differentiated due to overlapping. As shown in Fig. 1c, the characteristic absorption bands of WB and WB-g-PMAAc are still there, but weakened in the FTIR spectrum of the WB-g-PMAAc/CLI NC hydrogel, compared to the Fig. 1a, b. The peaks of carbonyl shifted to lower frequency. This may be because of the formation of hydrogen bonding between COOH and hydroxyl group of Al-OH and Si-OH in CLI. In addition; two bands at about 1,022 cm^{-1} are due to Si–O and 418 cm^{-1} related to Al–OH in the NC hydrogel (Al et al. 2008).

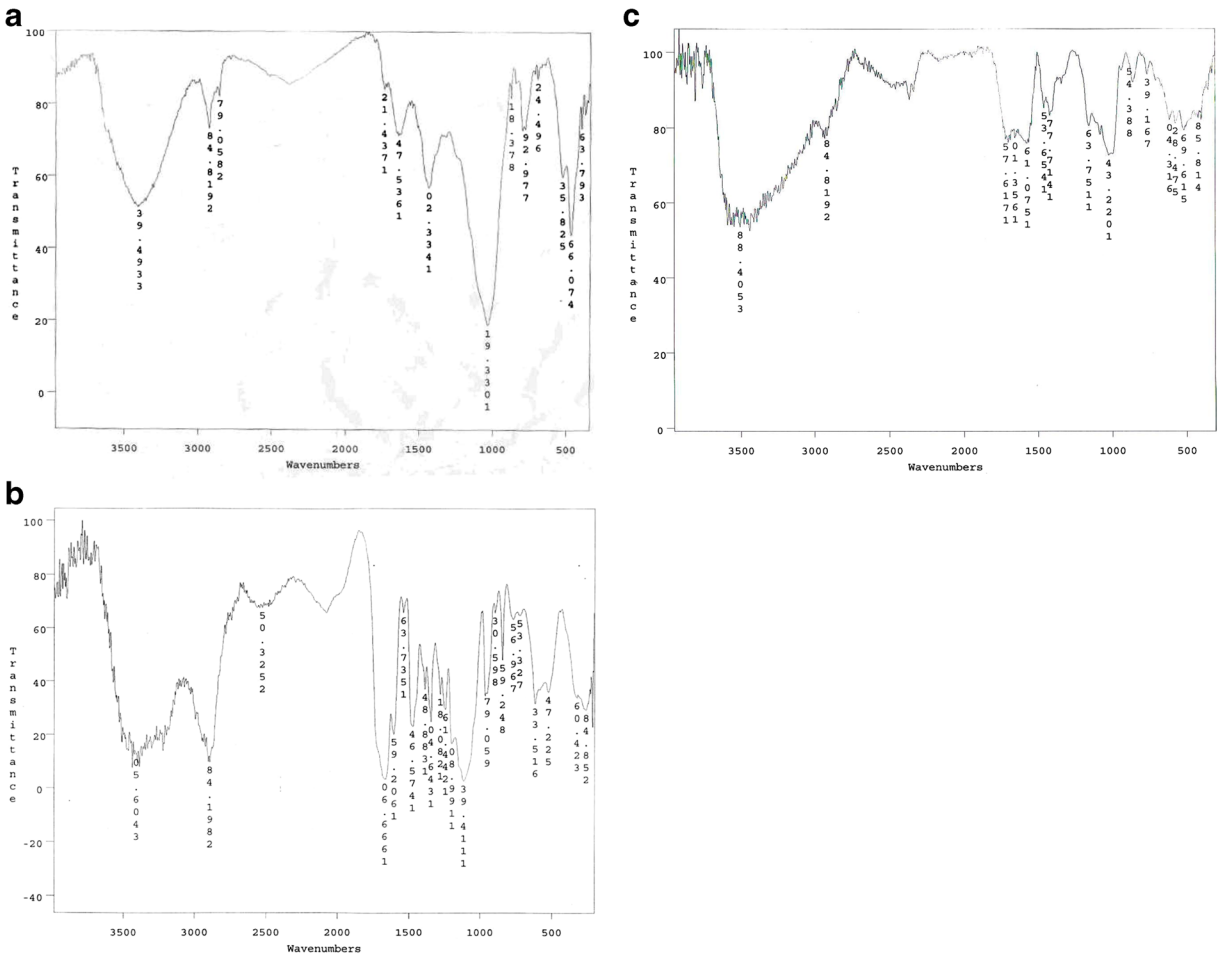

Fig. 1 FTIR spectra of **a** WB, **b** WB-g-PMAAc, and **c** WB-g-PMAAc/CLI

3.2 X-ray Diffraction Analysis

The XRD patterns of CLI and of WB-g-PMAAc/CLI NC hydrogel (containing 3 wt% CLI) are plotted in Fig. 2 in the spectral range of 2θ=2–25°. The corresponding d_{001} diffraction signal of the CLI was detected at 2θ=7.02°, correspondent to d_{001}=12.58 . This reflection intensity was reduced four times in the pattern of NC hydrogel, which indicated that exfoliation was occurred between CLI and matrix system. The d-spacing of CLI increased from 12.58 to 13.38 after polymerization, indicating the intercalation of CLI. Hence, a broad peak observed at 2θ=16° is due to polymer composite matrix (WB-g-PMAAc). This is in line with finding of Rashidzadeh and his co-workers who studied the swelling properties of hydrogel NC based on

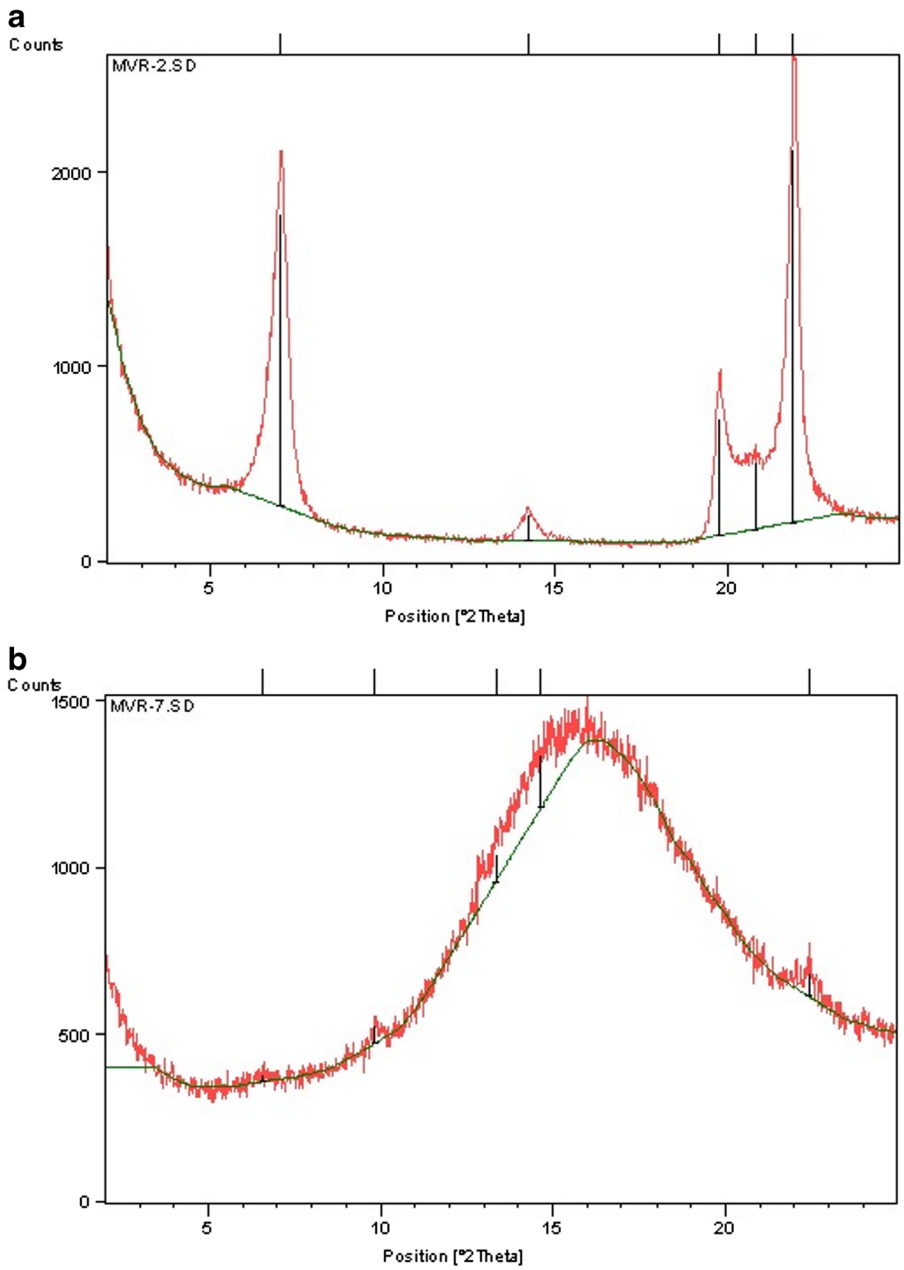

Fig. 2 X-ray diffraction patterns of **a** CLI and **b** WB-g-PMAAc/CLI

alginate-g-poly(acrylic acid-co-acrylamide)/CLI and its application as slow release fertilizer hydrogel. They concluded a similar result, due to the deposition of hydrogel on the outer and inner surfaces of CLI lattice channels, and the intensity of peaks was related to the CLI decreases (Rashidzadeh et al. 2014).

3.3 Scanning Electron Microscopy Analysis

The SEM micrographs of cross-linked WB-g-PMAAc and WB-g-PMAAc/CLI NC hydrogels containing 1 and 3 wt% are depicted in Fig. 3a–c, respectively, and after being swollen up to water equilibrium. It can be observed from Fig. 3a that the WB-g-PMAAc hydrogel only exhibits a smooth and dense surface, while the NC hydrogel which containing CLI shows a relatively coarse and undulant surface (Fig. 3b, c). The degree of dispersion of zeolite nanopowder in the polymer matrix is more important for an organic–inorganic NC. As shown in Fig. 3b, c, the CLI particles are more finely dispersed in the matrix, and no agglomeration of CLI particles was observed. Diffusion of water-bonded silicate toward the outside of matrix results in dispersion of CLI particles at the exterior surface of a porous polymer matrix after its immersion in water (Bortolin et al. 2013).

3.4 Thermogravimetric Analysis

In general, thermal decomposition of WB-g-PMAAc follows the processes that include desorption of physically adsorbed water, removal of structural water (dehydration reactions), scissions of C–O, and C–C bonds in the ring units resulting in the evolution of CO, CO_2, and H_2O and finally the formation of coke structures (Zhang et al. 2007b). From the TGA of WB-g-PMAAc and WB-g-PMAAc/CLI NC hydrogel (containing 3 wt% CLI), which are shown in Fig. 4a, b, respectively, it can be observed that the initial

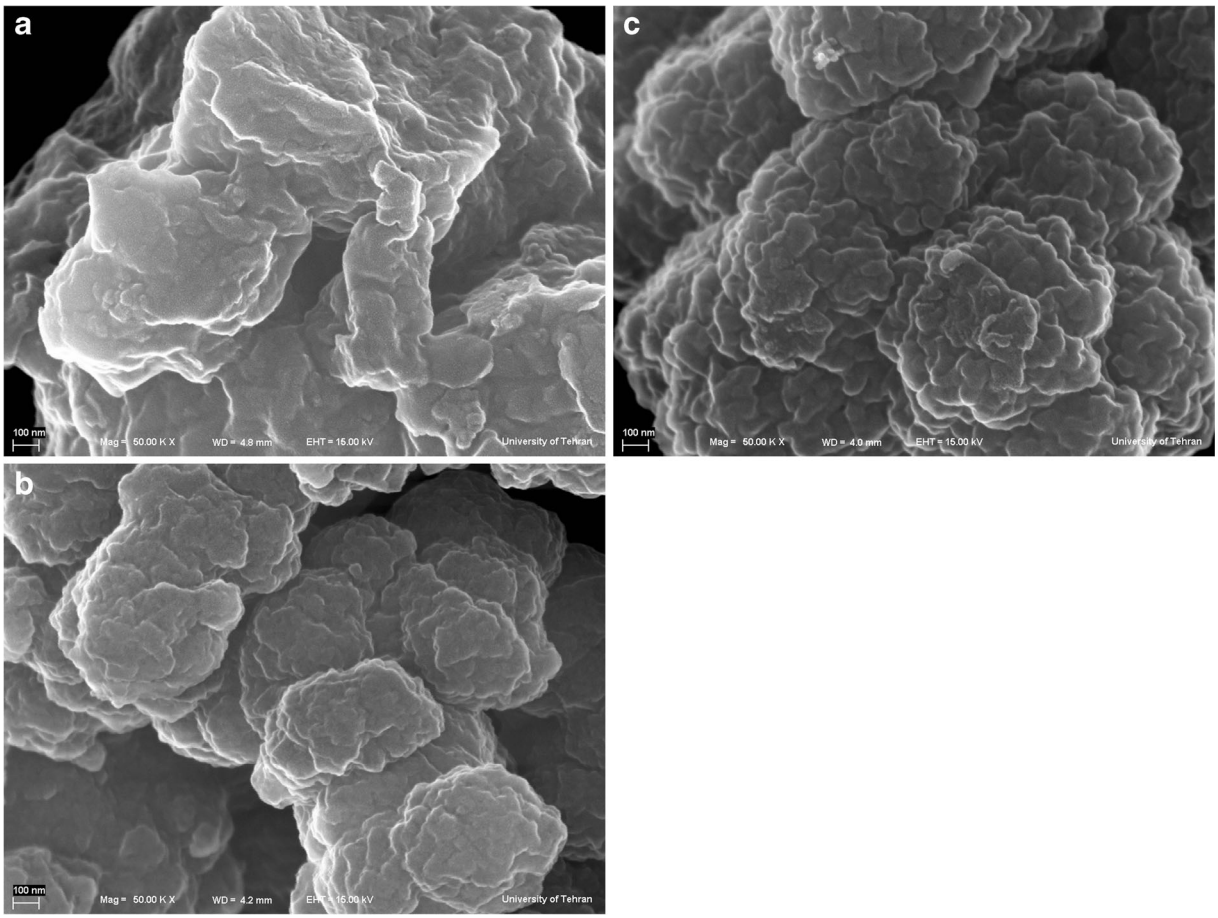

Fig. 3 Scanning electron micrographs of **a** WB-g-PMAAc, **b** WB-g-PMAAc/CLI (1 wt% of CLI), and **c** WB-g-PMAAc/CLI (3 wt% of CLI)

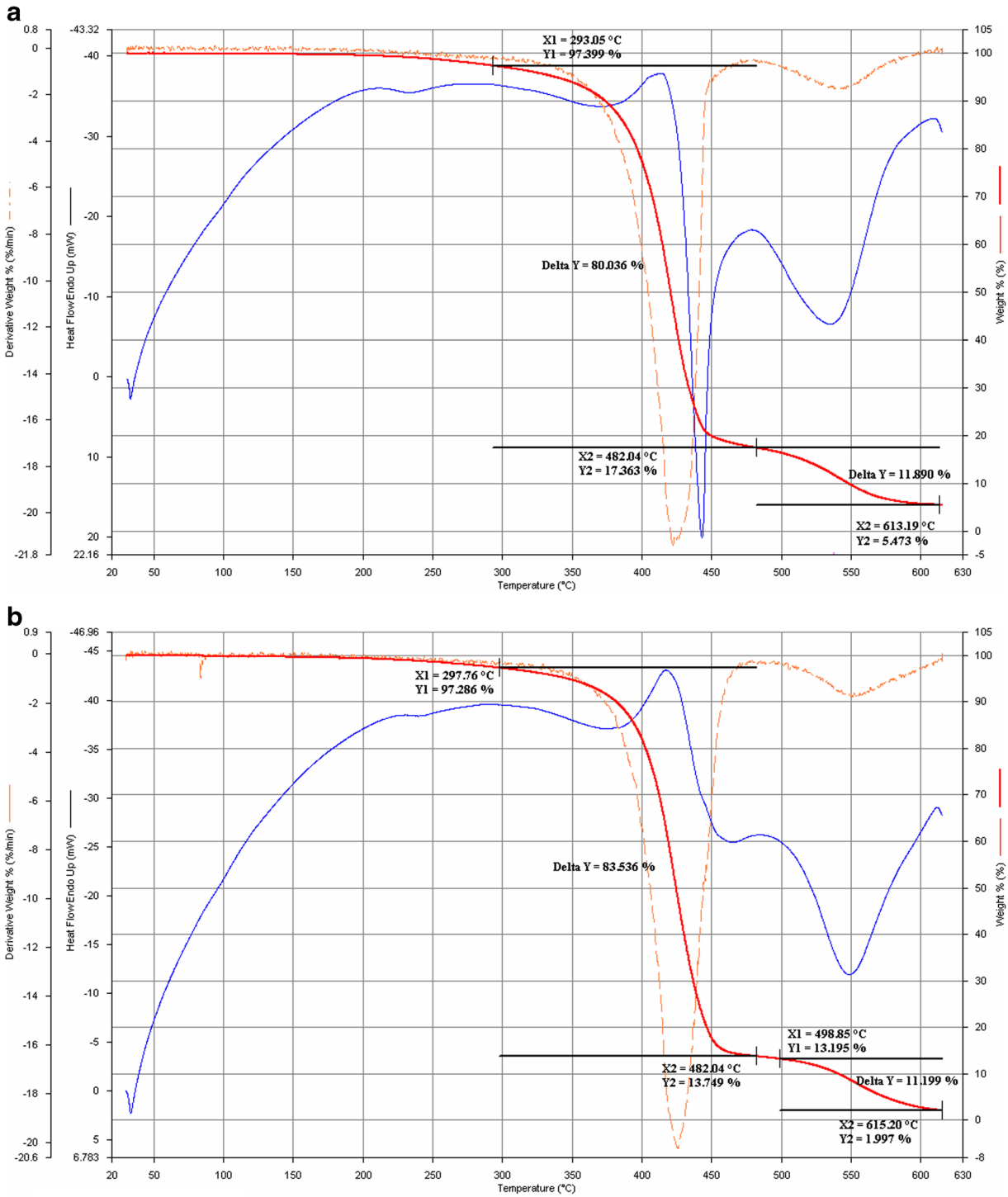

Fig. 4 TGA thermograms of **a** WB-g-PMAAc and **b** WB-g-PMAAc/CLI (3 wt% of CLI)

decomposition temperature was at 293.1 and 297.8 °C and final decomposition temperature was observed at 613.2 and 615.2 °C for WB-g-PMAAc and WB-g-PMAAc/CLI, respectively. The incorporation of CLI in WB-g-PMAAc matrix slightly increased the thermal stability of the formulation, i.e., WB-g-PMAAc/CLI NC

hydrogel. This can be attributed to the high thermal stability of the zeolites and to the interaction between the zeolite particles and the polymer matrix (Zhang et al. 2007a). Further, it is observed that maximum loss in cross-linked polymer occurred after the first stage of decomposition where the temperature range was usually corresponding to the depolymerization process. However, the proposed NC hydrogel is intended to be used for the adsorption of heavy metal cations from the aqueous solution, and the removal process is normally carried out at ambient temperature. Our test shows that the prepared NC polymer is totally stable in the ambient temperature.

3.5 Adsorption Capacity

Figure 5 shows the effect of contact time on the adsorption capacity of single metal solution. The same trend was observed for Pb(II), Cd(II), Cu(II), and Ni(II), where the initial stage is linear and indicated by a steep increase in capacity. The adsorption increases with time up to 60 min for Pb(II), Cd(II), and Cu(II) and up to 30 min for Ni(II) and then saturates. This rapid adsorption rate is consistent with results derived from the SEM analysis, which revealed NC hydrogels porous microstructure. This makes it more attractive for the solution accommodation.

The adsorption data at different initial cation concentrations is shown in Fig. 6. A higher initial metal ion concentration results in an increase in the diffusion of ions into the polymeric network as a result of an increase in the driving force, provided by the concentration gradient. However, by further increasing the initial concentration of cations (higher than 200 mg L^{-1}), the amount of ions adsorbed remains nearly constant due to saturation of the adsorption sites at the adsorbents. However, NC hydrogel can adsorb about 38.1, 33.4, 27.5, and 20.1 mg g^{-1} of Pb(II), Cd(II), Cu(II), and Ni(II), respectively.

Figure 7 shows the adsorption capacity of metal ions at different CLI levels in as-prepared NC hydrogel. The result shows that by increasing the CLI content from 0 to 5 wt%, the adsorption of cations increased by three to four times. According to the FTIR analysis, Fig. 1b, –OH bond of CLI participated in the copolymerization and the formation of the intercalated nanostructure in WB-g-PMAAc/CLI, which may improve the polymeric network strength and hence enhance the adsorption capacity. But, any further increase in CLI content of NC hydrogel had a negative effect on the adsorption of metal ions, and the adsorption capacity decreased by 1 to 1.5 times based on NC hydrogel with CLI content= 5 wt%. Because of –OH bond of hydrated CLI, interaction between CLI and neutralized MAAc became intensive. This means that more chemical and physical cross-link bonds were formed and elasticity of the polymer chains decreased. Consequently, the osmotic pressure between the polymeric network and the external solution for water permeation decreased which results in the lower adsorption capacity of WB-g-PMAAc/CLI NC. This is in line with finding of Wang and co-worker who studied the adsorption performance of chitosan-g-poly(acrylic acid)/montmorillonite NC hydrogels for methylene blue (MB) in which they concluded a similar result that an appropriate montmorillonite content was critical for improving the adsorption rate for MB (Wang et al. 2008).

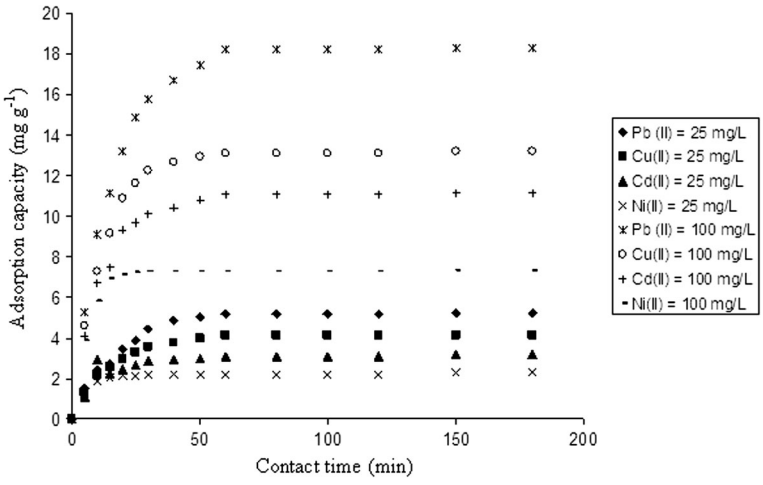

Fig. 5 Influences of contact time on the adsorption capacity of nanocomposite hydrogel for metal ions with different amounts of C_0 (pH=6.8, temperature=298 K, adsorbent dose=100 mg/100 mL, CLI content=3 wt%)

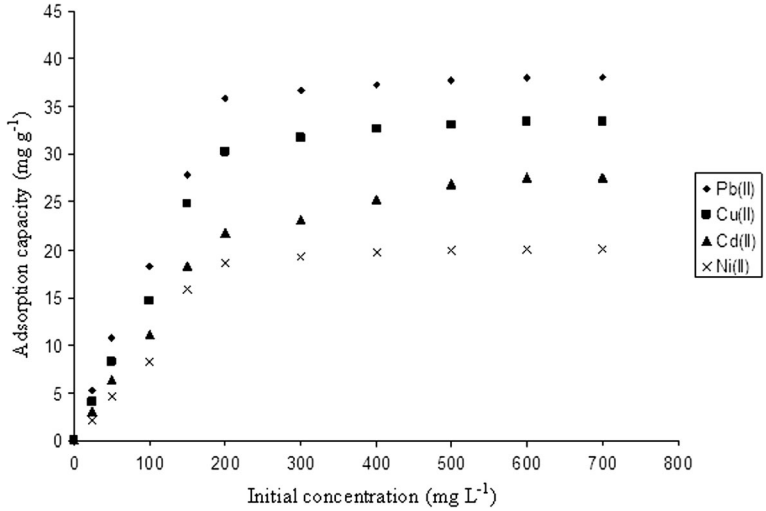

Fig. 6 Effect of cations initial concentration on adsorption capacity of nanocomposite hydrogel (contact time=60 min, pH=6.8, temperature=298 K, adsorbent dose=100 mg/100 mL, CLI content=3 wt%)

3.6 Adsorption Equilibrium Isotherms

The interaction between the adsorbate and the adsorbent was investigated by fitting the adsorption data (see Fig. 8a–d) to the Langmuir, Freundlich, Temkin, and Dubinin–Radushkevich (D-R) isotherm models.

The Langmuir isotherm is the simplest isotherm theoretical model and is valid for monolayer sorption due to a surface of a finite number of adsorption sites of uniform energies of adsorption with no transmigration of adsorbate in the plane of the surface. The Langmuir equation is expressed in the linear form as Eq. 2.

$$\frac{1}{q_e} = \frac{1}{bq_{max}C_e} + \frac{1}{q_{max}} \tag{2}$$

where q_e is the amount of adsorbed ions at equilibrium (mg g^{-1}), q_{max} is the monolayer adsorption capacity of the adsorbent (mg g^{-1}), C_e is the equilibrium concentration of ion solution (mg L^{-1}), and b is the Langmuir adsorption constant (L mg^{-1}) and is related to the free energy of adsorption.

The Freundlich expression describes the heterogeneous surface energies by multilayer adsorption and is expressed in a linear form as Eq. 3.

$$\log q_e = \log K_F + \frac{1}{n}\log C_e \tag{3}$$

where K_F includes adsorption extent (mg g^{-1}) and n is an empirical parameter related to the intensity of

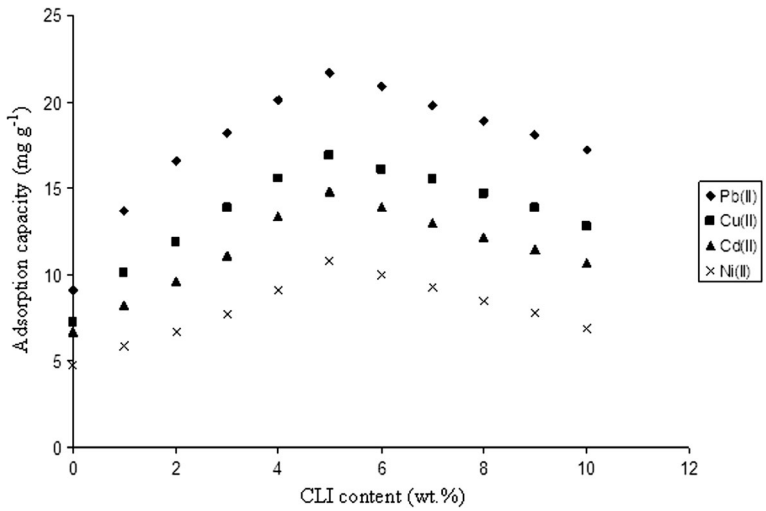

Fig. 7 Effect of clinoptilolite content on adsorption capacity of nanocomposite hydrogel (C_0=100 mg L^{-1}, pH=6.8, temperature=298 K, contact time=60 min, and adsorbent dose=100 mg/100 mL)

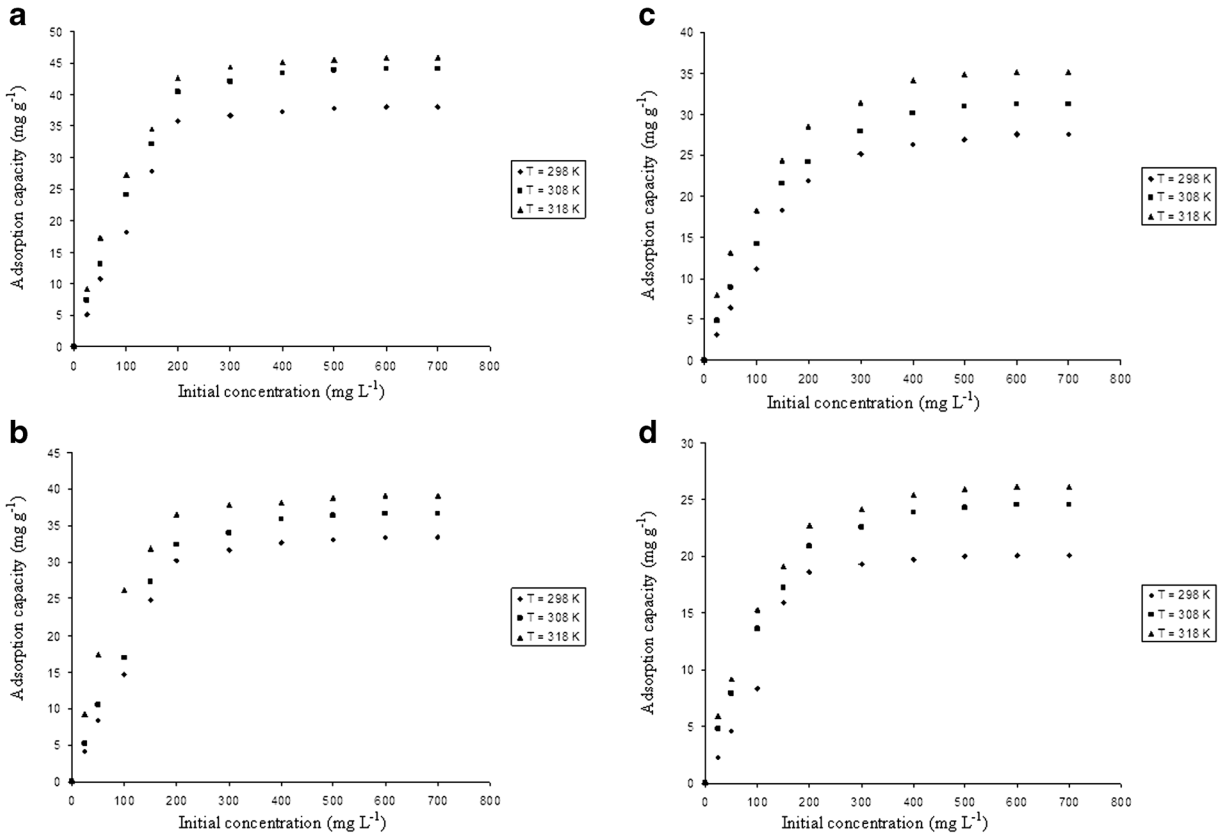

Fig. 8 Adsorption isotherms of **a** Pb^{2+}, **b** Cu^{2+}, **c** Cd^{2+}, and **d** Ni^{2+} on nanocomposite hydrogel at different temperatures (contact time= 60 min, pH=6.8, adsorbent dose=100 mg/100 mL, CLI content=3 wt%)

adsorption, which varies with the nonlinearity between solution concentration and adsorption.

The Temkin isotherm (Alyüz and Veli 2009) is an early model describing the adsorption of metal ions onto adsorbents. The isotherm contains a factor that explicitly takes into account the adsorbent–adsorbate interaction and is based on the assumption that the free energy of sorption is a function of the surface coverage. The Temkin isotherm in the linear form is expressed as follows:

$$q_e = \frac{RT}{b_T}\ln A_T + \left(\frac{RT}{b_T}\right)\ln C_e \tag{4}$$

where A_T is the equilibrium binding constant corresponding to the maximum binding energy (L mg^{-1}), b_T is the Temkin isotherm constant, T is the temperature (K), and R is the ideal gas constant (8.314 J mol^{-1} K^{-1}).

The D-R isotherm is more generally used to distinguish between physical and chemical adsorption and is given by the following equation (Argun et al. 2007):

$$\ln q_e = \ln q_{max} + K\varepsilon^2 \tag{5}$$

where ε is the Polanyi potential and equals to $RT\ln\left(1+\frac{1}{C_e}\right)$ and K is related to the mean free adsorption energy per mole of adsorbate, E (kJ mol^{-1}). E denotes the energy required to transfer 1 mole of fluoride to adsorbent sites from infinite in a solution medium. E provides information about chemical and physical adsorption (Nguyen and Do 2001) and can be obtained using the following relationship:

$$E = \frac{1}{\sqrt{-2K}} \tag{6}$$

The conformity between the experimental data and the model-predicted values was expressed by the

coefficient of determinations (R^2). R^2 values close or equal to 1 indicate that the model describes the isotherms of cation adsorption more accurately.

The isotherm constants and the determination coefficient, R^2, were calculated and summarized in Table 1. By comparing the linear regression values, it is clear that the Langmuir and Freundlich isotherms are capable of representing the data more satisfactory (R^2=0.98–0.99) than the Temkin and D-R isotherms (R^2=0.79–0.98). All of the investigated heavy metals in this study have high determination coefficient (R^2>0.99) with Langmuir isotherm. Pb(II) having the maximum b value at ambient temperature means the highest affinity to bind to the functional and pendant groups, resulting to maximum adsorption capacity over Cu(II), Cd(II), and Ni(II). The essential characteristics of the Langmuir isotherm (b) can be described by a dimensionless constant separation factor or equilibrium parameter, R_L, which is defined by Eq. 7 (Jin and Bai 2002):

$$R_L = \frac{1}{1 + bC_0} \tag{7}$$

where C_0 (mg L^{-1}) is the initial concentration of metal ion. The separation factor R_L indicates whether the isotherm is unfavorable (R_L<1 or R_L>1), linear (R_L=1), favorable (0<R_L<1), and irreversible (R_L=0) (Jin and Bai 2002). The R_L values at concentrations 25–600 mg L^{-1} (T=318 K) for Pb(II) (0.14–0.79), Cu(II) (0.11–0.79), Cd(II) (0.08–0.69), and Ni(II) (0.12–0.76) are between 0 and 1 indicating a highly favorable adsorption.

It is known that the magnitude of E is very common for evaluating the type of adsorption and if this value lies in between 8 and 16 kJ mol^{-1}, the adsorption can be explained by ion exchange (Guibal et al. 1998). As presented in Table 1, the E values of D-R isotherm obtained lie between 8.46 and 10.28 kJ mol^{-1}, indicating that ion exchange mechanism governs the metal ion uptake. According to Kamari and Wan Ngah (2009), ions with higher electronegativity are preferentially adsorbed. The electronegativity of Pb(II), Cd(II), Cu(II), and Ni(II) are 2.33, 1.90, 1.09, and 1.91, respectively, thus corroborating the adsorption profile of these metal ions.

3.7 Adsorption Kinetics

The two main types of sorption kinetic models, namely, reaction-based and diffusion-based models were adopted to fit the experimental data. These models also describe the solute uptake rate, and evidently, this rate controls the time of adsorbate uptake at NC hydrogel interface. Three kinetic models, namely, pseudo-first order, pseudo-second order, and interparticle diffusion were utilized to describe the adsorption rate of the model cations on the NC hydrogel and expressed as follows (Ho 2006):

Pseudo-first-order model,

$$\log(q_e - q_t) = \log q_e - \frac{k_1 t}{2.303} \tag{8}$$

Pseudo-second-order model,

$$\frac{t}{q_t} = \frac{1}{k_2 {q_e}^2} + \frac{t}{q_e} \tag{9}$$

Table 1 Parameters of kinetic models of metal cation adsorption onto nanocomposite hydrogel

Metal ion	C_i (mg L^{-1})	Pseudo-first order			Pseudo-second order			Interparticle diffusion		
		k_1 (min^{-1})	q_e^{th}	R^2	k_2 (g mg^{-1} min^{-1})	q_e^{th}	R^2	k_{id}	C_e	R^2
Pb^{2+}	25	0.0677	5.864	0.983	0.0073	6.998	0.991	0.6965	0.209	0.955
	100	0.0592	17.21	0.995	0.0028	23.04	0.997	2.2738	2.058	0.927
Cu^{2+}	25	0.0599	3.885	0.998	0.0137	5.118	0.999	0.4979	0.939	0.939
	100	0.0791	12.46	0.994	0.0062	15.698	0.994	1.4915	2.983	0.855
Cd^{2+}	25	0.0587	2.468	0.973	0.0293	3.609	0.997	0.3292	0.861	0.861
	100	0.0675	9.251	0.979	0.0081	12.953	0.997	1.1846	2.885	0.865
Ni^{2+}	25	0.1199	1.829	0.956	0.0869	2.569	0.993	0.2819	0.799	0.799
	100	0.1591	7.927	0.989	0.0221	8.741	0.992	1.0124	2.279	0.842

Interparticle diffusion model,

$$q_t = k_{id} t^{0.5} + C_i \quad (10)$$

where k_1 (mg g^{-1} min^{-1}) is the pseudo-first-order kinetic constant; k_2 (g mg^{-1} min^{-1}) is the pseudo-second-order kinetic constant; k_{id} (mg g^{-1} $min^{-0.5}$) is the interparticle diffusion kinetic constant; C_i is the thickness of the boundary layer (mm); and q_e is the amount of solute sorbed at equilibrium (mg g^{-1}), while q_t is the amount of solute sorbed at time t (mg g^{-1}) before reaching equilibrium.

Table 2 shows the kinetic constant as well as the determination coefficients, R^2. Based on the correlation coefficients, the adsorption of the cations is best described by the second-order equation. Table 2 data indicate that the q_e^{th} values for the second-order model are closer to q_e^{exp} values (6.998, 5.118, 3.609, and 2.569 mg g^{-1} for Pb(II), Cd(II), Cu(II), and Ni(II), respectively, for C_0=25 mg L^{-1}) in comparison to first-order values. Therefore, it can be concluded that the cation sorption on to the NC hydrogel seems to be dominantly pseudo-second order. This means that the chemisorption is the rate-controlling mechanism for adsorption of the cations to the studied adsorbents.

3.8 Effect of Temperature on Metal Cation Adsorption

The adsorption behavior of NC hydrogel is affected by the temperature of the adsorption medium in many ways. With increasing the temperature, the adsorption of heavy metal ions increased (shown in Fig. 9a–d). This reveals the endothermic nature of the adsorption (Zhao et al. 2010). The increase in the temperature of the adsorption medium is usually accompanied by the enhancement of the solution intake rate due to increased kinetic energy of solvent molecules. The activation energy of the solution intake process (swelling process) was determined by fitting the experimental data to the Arrhenius equation given below:

$$\ln k = \ln(A) - \left(\frac{E_a}{RT}\right) \quad (11)$$

where E_a (J mol^{-1}) is the apparent activation energy for the adsorption process, k the rate constant (s^{-1}), A the Arrhenius constant (s^{-1}), R the gas constant (8.314 J mol^{-1} K^{-1}), and T (K) is the solution temperature. The activation energies for the NC hydrogel (determined from the slope of the linear plot between the logarithm of k (k_2; Table 3) and $1/T$ (see Fig. 10)) have been found to be 16.8, 22.2, 23.1, and 28.1 kJ mol^{-1} for Pb(II), Cd(II), Cu(II), and Ni(II), respectively. It is known that the magnitude of E_a is very common for evaluating the type of adsorption. Some of the assigned values of E_a (kJ mol^{-1}) include 8.0–25.0 to physical adsorption, less than 21.0 to aqueous diffusion, and 20–40 to pore diffusion (Wu et al. 2012). It was obtained from this result that the adsorption involved both physical adsorption and pore diffusion processes.

Table 2 Estimated adsorption isotherm parameters for metal cation adsorption

Metal ion	Temperature (K)	Langmuir			Freundlich			Temkin			D-R		
		q_{max}	$b\times10^3$	R^2	K_F	n	R^2	A_T	b_T	R^2	q_{max}	$K\times10^{10}$	R^2
Pb^{2+}	298	166.7	1.64	0.996	0.374	1.118	0.995	0.062	177.7	0.936	25.2	−1.1	0.837
	308	76.3	6.06	0.997	0.823	1.297	0.999	0.079	173.5	0.961	29.4	−0.7	0.811
	318	66.7	10.1	0.998	1.641	1.542	0.989	0.111	188.9	0.981	32.8	−0.5	0.867
Cu^{2+}	298	243.9	0.82	0.998	0.225	1.044	0.994	0.054	199.7	0.921	21.1	−1.3	0.808
	308	103.1	2.71	0.996	0.423	1.173	0.991	0.064	202.5	0.988	23.6	−1.0	0.831
	318	52.6	13.4	0.999	1.961	1.707	0.985	0.131	225.9	0.996	29.8	−0.4	0.875
Cd^{2+}	298	175.4	0.83	0.997	0.177	1.068	0.995	0.054	277.3	0.937	15.7	−1.4	0.828
	308	48.5	5.42	0.998	0.509	1.322	0.993	0.072	280.5	0.958	18.6	−0.9	0.831
	318	34.4	17.3	0.992	1.729	1.836	0.994	0.129	304.3	0.969	22.3	−0.5	0.823
Ni^{2+}	298	166.6	0.57	0.997	0.082	0.954	0.989	0.046	308.9	0.902	12.7	−1.7	0.796
	308	31.6	8.68	0.994	0.629	1.472	0.998	0.082	349.1	0.973	15.9	−0.8	0.815
	318	31.6	11.9	0.998	1.087	1.691	0.992	0.108	359.9	0.986	18.1	−0.6	0.863

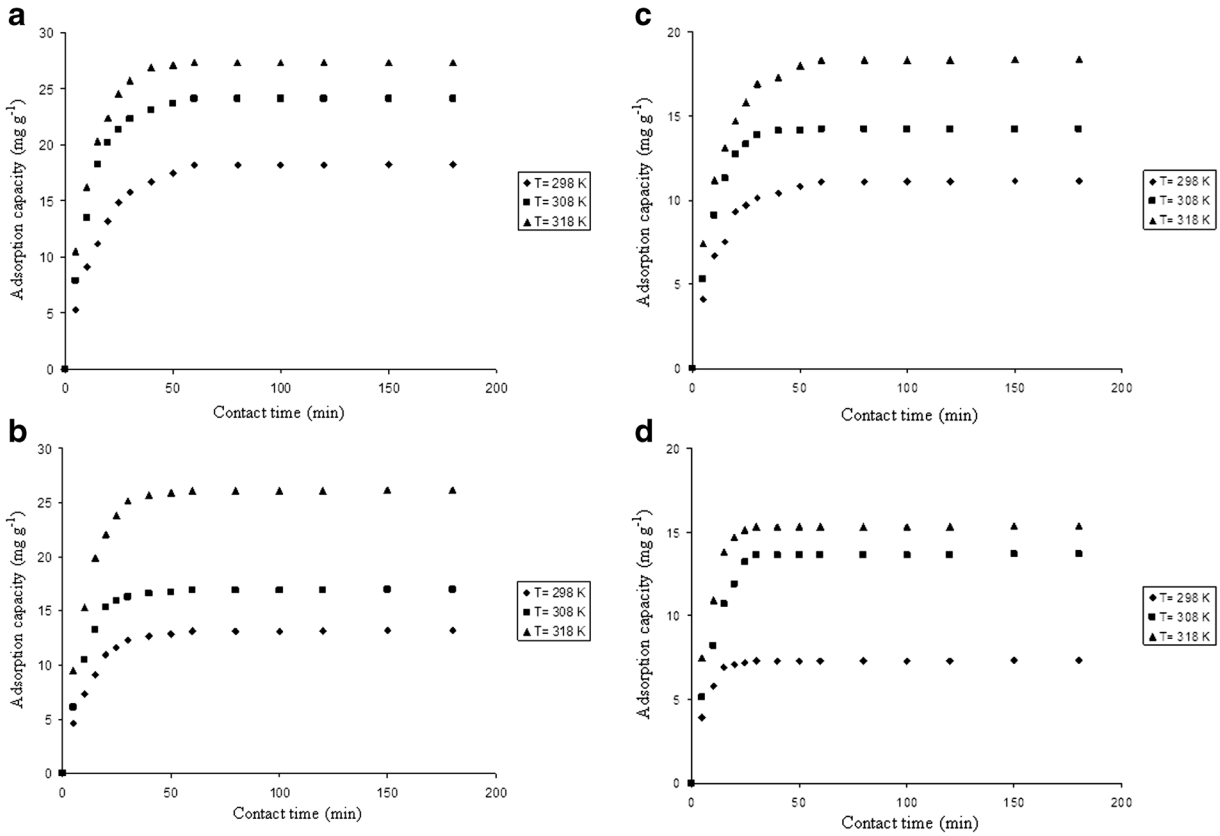

Fig. 9 Effect of temperature on the adsorption capacity of nanocomposite hydrogel for **a** Pb^{2+}, **b** Cu^{2+}, **c** Cd^{2+}, and **d** Ni^{2+} (C_0=100 mg L^{-1}, pH=6.8, adsorbent dose=100 mg/100 mL, CLI content=3 wt%)

The variation in the extent of adsorption with respect to the temperature has also been explained on the basis of thermodynamic parameters. The free energy (ΔG^0), enthalpy (ΔH^0), and entropy (ΔS^0) change for the

Table 3 Parameters of kinetic models of metal cation adsorption onto nanocomposite hydrogel in different solution temperatures

Metal ion	Temperature (K)	Pseudo-first order			Pseudo-second order			Interparticle diffusion		
		k_1 (min^{-1})	q_e^{th}	R^2	k_2 (g mg^{-1} min^{-1})	q_e^{th}	R^2	k_{id}	C_e	R^2
Pb^{2+}	298	0.0592	17.21	0.995	0.0028	23.04	0.997	2.2738	2.058	0.927
	308	0.0782	26.98	0.965	0.0034	28.81	0.992	2.1757	5.693	0.825
	318	0.1025	31.75	0.992	0.0043	32.05	0.996	10.098	−22.6	0.974
Cu^{2+}	298	0.0791	12.46	0.994	0.0062	15.69	0.994	1.4915	2.983	0.855
	308	0.0953	14.58	0.984	0.0087	19.56	0.991	1.7643	5.292	0.758
	318	0.1232	28.54	0.995	0.0109	30.77	0.993	2.8532	7.124	0.816
Cd^{2+}	298	0.0675	9.251	0.979	0.0081	12.95	0.997	1.1846	2.885	0.865
	308	0.0995	14.15	0.991	0.0111	16.39	0.991	1.4579	4.655	0.763
	318	0.1345	20.71	0.955	0.0145	21.19	0.999	1.8821	5.259	0.891
Ni^{2+}	298	0.1591	7.927	0.989	0.0221	8.74	0.992	1.0124	2.279	0.842
	308	0.1704	23.81	0.893	0.0321	20.75	0.995	2.6824	−0.37	0.974
	318	0.1856	21.29	0.978	0.0451	19.53	0.992	2.4473	3.004	0.905

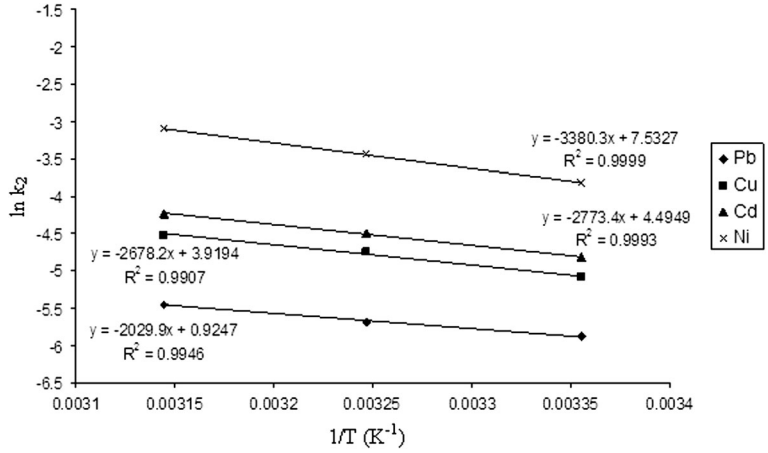

Fig. 10 Plot of pseudo-second-order kinetic constant (ln k_2) vs. temperature ($1/T$). The activation energies of the adsorption process are determined from this *graph*

interaction of the cations–NC hydrogel was evaluated by using the following equation (Chen et al. 2010):

$$\Delta G^0 = RT\ln b \tag{12}$$

$$\frac{d\ln b}{dT} = \frac{\Delta H^0}{RT^2} \tag{13}$$

$$\Delta G^0 = \Delta H^0 - T\Delta S^0 \tag{14}$$

It is obvious that the negative values of free energy change (ΔG^0), as shown in Table 4, were an indication of feasible and spontaneous nature of the adsorption process. The positive values of ΔH^0 suggest the endothermic nature of the process. The positive values of the ΔS^0 show the increased randomness at the solid–solution interface during the adsorption process and also reflect the affinity of the adsorbent material for the metal ions under consideration (Ai et al. 2011).

Table 4 Thermodynamic parameters of metal cation adsorption onto nanocomposite hydrogel in different solution temperatures

Metal ion	Temperature (K)	ΔG^0 (kJ mol^{-1})	ΔH^0 (kJ mol^{-1})	ΔS^0 (kJ mol^{-1} K^{-1})
Pb^{2+}	298	−15.88	72.03	56.15
	308	−13.08		58.96
	318	−12.13		59.90
Cu^{2+}	298	−17.59	109.71	92.11
	308	−15.14		94.56
	318	−11.39		98.31
Cd^{2+}	298	−17.58	119.12	102.33
	308	−13.36		106.55
	318	−10.73		109.18
Ni^{2+}	298	−12.77	26.36	13.58
	308	−12.15		14.21
	318	−11.69		14.66

3.9 Effect of pH on Metal Cation Adsorption

The anionic feature and adsorption capacity of hydrogel strongly affects by variation in pH. This effect can be seen from Fig. 11 that the adsorption capacity of Pb(II) increased from 3.4 to 18.2 mg g^{-1} when pH of solution media increased from 2.1 to 6.8, but further increase of pH from 6.8 to 11.5 decreased the adsorption capacity of metal ions. This is because when the pH of the medium is low (pH=2), the carboxylic groups of poly(sodium methacrylate) are almost in an undissociated state, and therefore, these polymeric chains are closely packed through hydrogen bonding. When pH of the adsorbing medium increases from pH=2, the carboxylic groups dissociate into COO^- and result in relaxation of the networks by breaking the hydrogen bonds. Also, in this situation, more mobile ions (Na^+ ions) exist in the hydrogel which may make the ion exchange reaction between metal ions and exchangeable cations existing in the composite easy. This in turn increases the diffusion of water molecules into the network, therefore, increasing the adsorbing capacity. When the pH of the adsorbing medium is greater than 7, where the number of carboxylate anions reaches the maximum level, no more repulsion could be expected in the cross-linked hydrogel. This causes expulsion of water molecules

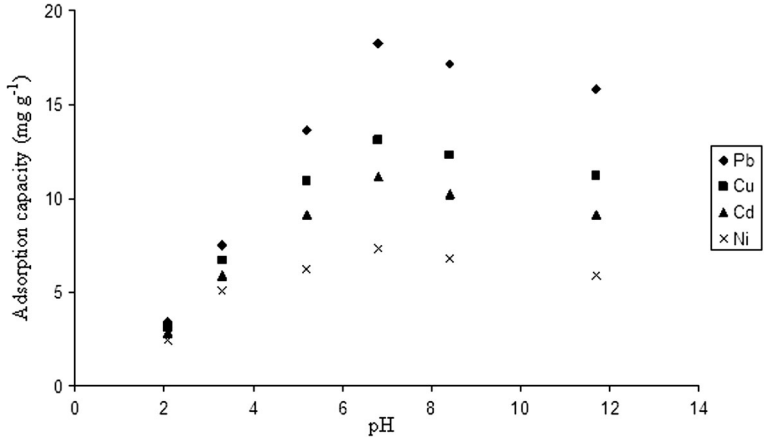

Fig. 11 Effects of pH on adsorption capacity of nanocomposite hydrogel for metal cations (C_0=100 mg L^{-1}, contact time=60 min, temperature=298 K, adsorbent dose=100 mg/100 mL, CLI content=3 wt%)

from within the hydrogel into the media due to the weakening of the hydrogen bonds formed between water molecules and cross-linked hydrogel chains. The formation of metal hydroxide (i.e., $Pb(OH)_2$ or $Cu(OH)_2$) precipitation is another cause, but with the same importance of the decrease in the adsorbing capacity when the pH value of adsorbing medium is in the alkaline range (Li and Bai 2005).

3.10 Desorption and Regeneration Study

Desorption studies are necessary in order to elucidate the nature of the adsorption process of metal ions onto NC hydrogels. Desorption of Pb(II), Cd(II), Cu(II), and Ni(II) was obtained using 1 mol L^{-1} HCl solution (Wang et al. 2009; Kamari and Wan Ngah 2009) with desorption ratios of 96, 96.5, 98, and 98 %, respectively.

Reusability of an adsorbent by a regeneration process is an important parameter. In this study, adsorption–desorption cycles of metal ions were repeated five times using the same adsorbent. Figure 12 shows the adsorption capacities of the adsorbents for metal ions over five successive adsorption–desorption cycles. It can be observed that the adsorption capacity of the adsorbents slightly decreased with an increase in adsorption–desorption cycles. As shown in Fig. 12, more than 90 % of the initial adsorption capacities were obtained after fifth cycle of desorption for the metal ions. Therefore, WB-g-PMAAc/CLI NC hydrogel is a good reusable adsorbent and could be successfully utilized for the recovery of heavy metal ions from water and/or wastewater.

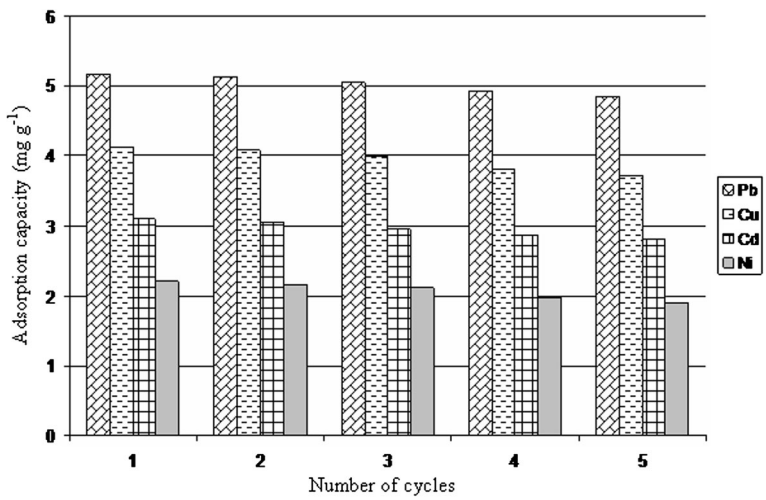

Fig. 12 Regeneration studies of WB-g-PMAAc/CLI after five cycles

4 Conclusions

This study has shown that the novel WB-g-PMAAc/CLI NC hydrogel can be an extremely viable adsorbent for application in the remediation of metal ions in industry effluent due to its excellent and attractive features such as nontoxic and good chemical stability and high capacity and rate of adsorption, and reusability. It should be noted that introduction of CLI and WB reduces the production cost of the adsorbent. Some important factors such as solution pH, contact time, initial metal concentration, and temperature were studied. The equilibrium capacity of metal cations correlated well with the Langmuir isotherm model, while the pseudo-second-order kinetic model showed the best fit to the kinetic data. Thermodynamic studies indicated that the adsorption process was feasible, spontaneous, and endothermic. The high adsorption capacity and average desorption efficiency during the consecutive five-time adsorption–desorption processes of WB-g-PMAAc/CLI NC hydrogel implied that the NC hydrogel possesses the potential of regeneration and reuse.

Acknowledgments The authors thank the Arak University research fund for providing financial support of this work.

References

Ai, L., Li, M., & Lif, L. (2011). Adsorption of methylene blue from aqueous solution with activated carbon/cobalt ferrite/alginate composite beads: kinetics, isotherms, and thermodynamics. *Journal of Chemical & Engineering Data, 56*(8), 3475–3483.

Akbal, F., & Camc, S. (2011). Copper, chromium and nickel removal from metal plating waste water by electrocoagulation. *Desalination, 269*(1–3), 214–222.

Al, E., Güçlü, G., İyim, T. B., Emik, S., & Özgümüş, S. (2008). Synthesis and properties of starch-graft-acrylic acid/Na-montmorillonite superabsorbent nanocomposite hydrogels. *Journal of Applied Polymer Science, 109*(1), 16–22.

Alyüz, B., & Veli, S. (2009). Kinetics and equilibrium studies for the removal of nickel and zinc from aqueous solutions by ion exchange resins. *Journal of Hazardous Materials, 167*(1–3), 482–488.

Argun, M. E., Dursun, S., Ozdemir, C., & Karatas, M. (2007). Heavy metal adsorption by modified oak sawdust: thermodynamics and kinetics. *Journal of Hazardous Materials, 141*(1), 77–85.

Bannon, D. I., Drexler, J. W., Fent, G. M., Casteel, S. W., Hunter, P. J., Brattin, W. J., & Major, M. A. (2009). Evaluation of small arms range soils for metal contamination and lead bioavailability. *Environmental Science & Technology, 43*(24), 9071–9076.

Barati, A., Norouzi, H., Sharafoddinzadeh, S., & Davarnejad, R. (2010). Swelling kinetics modeling of cationic methacrylamide-based hydrogels. *World Applied Sciences Journal, 11*(11), 1336–1341.

Barati, A., Asgari, M., Miri, T., & Eskandari, Z. (2013). Removal and recovery of copper and nickel ions from aqueous solution by poly(methacrylamide-co-acrylic acid)/ montmorillonite nanocomposites. *Environmental Science and Pollution Research, 20*(9), 6242–6255.

Bhardwaj, D., Sharma, M., Sharma, P., & Tomar, R. (2012). Synthesis and surfactant modification of clinoptilolite and montmorillonite for the removal of nitrate and preparation of slow release nitrogen fertilizer. *Journal of Hazardous Materials, 227–228*, 292–300.

Bortolin, A., Aouada, F. A., Mattoso, L. H. C., & Ribeiro, C. (2013). Nanocomposite PAAm/methyl cellulose/montmorillonite hydrogel: evidence of synergistic effects for the slow release of fertilizers. *Journal of Agricultural and Food Chemistry, 61*(31), 7431–7439.

Chen, M., Chen, Y., & Diao, G. (2010). Adsorption kinetics and thermodynamics of methylene blue onto *p-tert*-butyl-calix[4,6,8]arene-bonded silica gel. *Journal of Chemical & Engineering Data, 55*(11), 5109–5116.

Demirbilek, C., & Özdemir Dinç, C. (2012). Synthesis of diethylaminoethyl dextran hydrogel and its heavy metal ion adsorption characteristics. *Carbohydrate Polymers, 90*(2), 1159–1167.

Dupont, L., & Guillon, E. (2003). Removal of hexavalent chromium with a lignocellulosic substrate extracted from wheat bran. *Environmental Science & Technology, 37*(18), 4235–4241.

Futalan, C. M., Kan, C., Dalida, M. L., Hsien, K., Pascua, C., & Wan, M. (2011). Comparative and competitive adsorption of copper, lead and nickel using chitosan immobilized on bentonite. *Carbohydrate Polymers, 83*(2), 528–536.

Ghaee, A., Shariaty-Niassar, M., Barzin, J., & Zarghan, A. (2012). Adsorption of copper and nickel ions on macroporous chitosan membrane: equilibrium study. *Applied Surface Science, 258*(19), 7732–7743.

Giannopoulou, I., & Panias, D. (2007). Copper and nickel recovery from acidic polymetallic aqueous solutions. *Minerals Engineering, 20*(8), 753–760.

Guibal, E., Milot, C., & Tobin, J. M. (1998). Metal-anion sorption by chitosan beads: equilibrium and kinetic studies. *Industrial & Engineering Chemistry Research, 37*(4), 1454–1463.

Gupta, V. K., & Rastogi, A. (2009). Biosorption of hexavalent chromium by raw and acid-treated green alga *Oedogonium hatei* from aqueous solutions. *Journal of Hazardous Materials, 163*(1), 396–402.

Gupta, V. K., Mittal, A., Kurup, L., & Mittal, J. (2006a). Adsorption of a hazardous dye, erythrosine, over hen feathers. *Journal of Colloid and Interface Science, 304*(1), 52–57.

Gupta, V. K., Mittal, A., Kurup, L., & Mittal, J. (2006b). Adsorption treatment and recovery of the hazardous dye, Brilliant Blue FCF, over bottom ash and de-oiled soya. *Journal of Colloid and Interface Science, 293*(1), 16–26.

Gupta, V. K., Ali, I., & Saini, V. K. (2007a). Defluoridation of wastewaters using waste carbon slurry. *Water Research, 41*(15), 3307–3316.

Gupta, V. K., Jain, R., Mittal, A., Mathur, M., & Sikarwar, S. (2007b). Photochemical degradation of the hazardous dye Safranin-T using TiO_2 catalyst. *Journal of Colloid and Interface Science, 309*(2), 464–469.

Gupta, V. K., Jain, R., & Varshney, S. (2007c). Electrochemical removal of the hazardous dye Reactofix Red 3 BFN from industrial effluents. *Journal of Colloid and Interface Science, 312*(2), 292–296.

Gupta, V. K., Jain, R., & Varshney, S. (2007d). Removal of Reactofix golden yellow 3 RFN from aqueous solution using wheat husk—an agricultural waste. *Journal of Hazardous Materials, 142*(1–2), 443–448.

Gupta, V. K., Mittal, A., Malviya, A., & Mittal, J. (2009). Adsorption of carmoisine A from wastewater using waste materials—bottom ash and deoiled soya. *Journal of Colloid and Interface Science, 335*(1), 24–33.

Gupta, V. K., Rastogi, A., & Nayak, A. (2010). Biosorption of nickel onto treated alga (*Oedogonium hatei*): application of isotherm and kinetic models. *Journal of Colloid and Interface Science, 342*(2), 533–539.

Gupta, V. K., Agarwal, S., & Saleh, T. (2011a). Chromium removal by combining the magnetic properties of iron oxide with adsorption properties of carbon nanotubes. *Water Research, 45*(6), 2207–2212.

Gupta, V. K., Agarwal, S., & Saleh, T. (2011b). Synthesis and characterization of alumina-coated carbon nanotubes and their application for lead removal. *Journal of Hazardous Materials, 185*(1), 17–23.

Gupta, V. K., Gupta, B., Rastogi, A., Agarwal, S., & Nayak, A. (2011c). A comparative investigation on adsorption performances of mesoporous activated carbon prepared from waste rubber tire and activated carbon for a hazardous azo dye—Acid Blue 113. *Journal of Hazardous Materials, 186*(1), 891–901.

Gupta, V. K., Ali, I., Saleh, T., Nayak, A., & Agarwal, S. (2012). Chemical treatment technologies for waste-water recycling—an overview. *RSC Advances, 2*(16), 6380–6388.

Ho, Y.-S. (2006). Review of second-order models for adsorption systems. *Journal of Hazardous Materials, 136*(3), 681–689.

Hou, H., Zhou, R., Wu, P., & Wu, L. (2012). Removal of Congo red dye from aqueous solution with hydroxyapatite/chitosan composite. *Chemical Engineering Journal, 211–212*, 336–342.

Hua, S., Yang, H., Wang, W., & Wang, A. (2010). Controlled release of ofloxacin from chitosan–montmorillonite hydrogel. *Applied Clay Science, 50*(1), 112–117.

Huang, T., Xu, H. G., Jiao, K. X., Zhu, L. P., Brown, H. R., & Wang, H. L. (2007). A novel hydrogel with high mechanical strength: a macromolecular microsphere composite hydrogel. *Advanced Materials, 19*(12), 1622–1626.

Jain, A. K., Gupta, V. K., Bhatnagar, A., & Suhas. (2003). A comparative study of adsorbents prepared from industrial wastes for removal of dyes. *Separation Science and Technology, 38*(2), 463–481.

Jain, A. K., Gupta, V. K., Jain, S., & Suhas. (2004). Removal of chlorophenols using industrial wastes. *Environmental Science & Technology, 38*(4), 1195–1200.

Jin, L., & Bai, R. (2002). Mechanisms of lead adsorption on chitosan/PVA hydrogel beads. *Langmuir, 18*(25), 9765–9770.

Jovanović, Ž., Krklješ, A., Stojkovska, J., Tomić, S., Obradović, B., Mišković-Stanković, V., & Kačarević-Popović, Z. (2011). Synthesis and characterization of silver/poly(*N*-vinyl-2-pyrrolidone) hydrogel nanocomposite obtained by *in situ* radiolytic method. *Radiation Physics and Chemistry, 80*(11), 1208–1215.

Kamari, A., & Wan Ngah, W. S. (2009). Isotherm, kinetic and thermodynamic studies of lead and copper uptake by H_2SO_4 modified chitosan. *Colloids and Surfaces B: Biointerfaces, 73*(2), 257–266.

Karthikeyan, S., Gupta, V. K., Boopathy, R., Titus, A., & Sekaran, G. (2012). A new approach for the degradation of high concentration of aromatic amine by heterocatalytic Fenton oxidation: kinetic and spectroscopic studies. *Journal of Molecular Liquids, 173*, 153–163.

Kayaalt, Z., Mergen, G., & Söylemezoğlu, T. (2010). Effect of metallothionein core promoter region polymorphism on cadmium, zinc and copper levels in autopsy kidney tissues from a Turkish population. *Toxicology and Applied Pharmacology, 245*(2), 252–255.

Lara, R., Wuilloud, R., Salonia, J., Olsina, R., & Martinez, L. (2001). Determination of Low cadmium concentrations in wine by on-line preconcentration in a knotted reactor coupled to an inductively coupled plasma optical emission spectrometer with ultrasonic nebulization. *Fresenius' Journal of Analytical Chemistry, 371*(7), 989–993.

Lee, K.-Y., & Kim, K.-W. (2010). Heavy metal removal from shooting range soil by hybrid electrokinetics with bacteria and enhancing agents. *Environmental Science & Technology, 44*(24), 9482–9487.

Lee, M. H., Lee, S. W., Kim, S. H., Kang, C., & Kim, J. S. (2009). Nanomolar Hg(II) detection using Nile blue chemodosimeter in biological media. *Organic Letters, 11*(10), 2101–2104.

Li, N., & Bai, R. (2005). A novel amine-shielded surface cross-linking of chitosan hydrogel beads for enhanced metal adsorption performance. *Industrial & Engineering Chemistry Research, 44*(17), 6692–6700.

Li, P., Kim, N. H., Hui, D., Rhee, K. Y., & Lee, J. H. (2009). Improved mechanical and swelling behavior of the composite hydrogels prepared by ionic monomer and acid-activated laponite. *Applied Clay Science, 46*(4), 414–417.

Limparyoon, N., Seetapan, N., & Kiatkamjornwong, S. (2011). Acrylamide/2-acrylamido-2-methylpropane sulfonic acid and associated sodium salt superabsorbent copolymer nanocomposites with mica as fire retardants. *Polymer Degradation and Stability, 96*(6), 1054–1063.

Matz, C. J., & Krone, P. H. (2007). Cell death, stress-responsive transgene activation, and deficits in the olfactory system of larval zebrafish following cadmium exposure. *Environmental Science & Technology, 41*(14), 5143–5148.

Max Roundhill, D. (2004). Novel strategies for the removal of toxic metals from soils and waters. *Journal of Chemical Education, 81*(2), 275–283.

Mittal, A., Kurup, L., & Gupta, V. K. (2005). Use of waste materials—bottom ash and de-oiled soya, as potential adsorbents for the removal of Amaranth from aqueous solutions. *Journal of Hazardous Materials, 117*(1), 171–178.

Mittal, A., Gupta, V. K., Malviya, A., & Mittal, J. (2008). Process development for the batch and bulk removal and recovery of a hazardous, water-soluble azo dye (Metanil Yellow) by adsorption over waste materials (bottom ash and de-oiled soya). *Journal of Hazardous Materials, 151*(2–3), 821–832.

Mittal, A., Mittal, J., Malviya, A., & Gupta, V. K. (2010a). Removal and recovery of Chrysoidine Y from aqueous solutions by waste materials. *Journal of Colloid and Interface Science, 344*(2), 497–507.

Mittal, A., Mittal, J., Malviya, A., Kaur, D., & Gupta, V. K. (2010b). Adsorption of hazardous dye crystal violet from wastewater by waste materials. *Journal of Colloid and Interface Science, 343*(2), 463–473.

Molinari, R., Poerio, T., & Argurio, P. (2008). Selective separation of copper (II) and nickel (II) from aqueous media using the complexation–ultrafiltration process. *Chemosphere, 70*(3), 341–348.

Nguyen, C., & Do, D. D. (2001). The Dubinin-Radushkevich equation and the underlying microscopic adsorption description. *Carbon, 39*, 1327–1336.

Nüket Tirtom, V., Dinçer, A., Becerik, S., Aydemir, T., & Çelik, A. (2012). Comparative adsorption of Ni(II) and Cd(II) ions on epichlorohydrin crosslinked chitosan–clay composite beads in aqueous solution. *Chemical Engineering Journal, 197*, 379–386.

Pośpiech, B., & Walkowiak, W. (2007). Separation of copper(II), cobalt(II) and nickel(II) from chloride solutions by polymer inclusion membranes. *Separation and Purification Technology, 57*(3), 461–465.

Pourbeyram, S., & Mohammadi, S. (2014). Synthesis and characterization of highly stable and water dispersible hydrogel–copper nanocomposite. *Journal of Non-Crystalline Solids, 402*, 58–63.

Pourjavadi, A., Ayyari, M., & Amini-Fazl, M. S. (2008). Taguchi optimized synthesis of collagen-g-poly(acrylic acid)/kaolin composite superabsorbent hydrogel. *European Polymer Journal, 44*(4), 1209–1216.

Qdais, H. A., & Moussa, H. (2004). Removal of heavy metals from wastewater by membrane processes: a comparative study. *Desalination, 164*(2), 105–110.

Ramachandra Reddy, B., & Neela Priya, D. (2005). Process development for the separation of copper(II), nickel(II) and zinc(II) from sulphate solutions by solvent extraction using LIX 84 I. *Separation and Purification Technology, 45*(2), 163–167.

Rashidzadeh, A., Olad, A., Salari, D., & Reyhanitabar, A. (2014). On the preparation and swelling properties of hydrogel nanocomposite based on sodium alginate-*g*-poly (acrylic acid-*co*-acrylamide)/clinoptilolite and its application as slow release fertilizer. *Journal of Polymer Research, 21*, 344–351.

Reis, A. V., Guilherme, M. R., Moia, T. A., Mattoso, L. H. C., Muniz, E. C., & Tambourgi, E. B. (2008). Synthesis and characterization of a starch-modified hydrogel as potential carrier for drug delivery system. *Journal of Polymer Science Part A: Polymer Chemistry, 46*(7), 2567–2574.

Salam, A., Pawlak, J. J., Venditti, R. A., & El-tahlawy, K. (2010). Synthesis and characterization of starch citrate−chitosan foam with superior water and saline absorbance properties. *Biomacromolecules, 11*(6), 1453–1459.

Saleh, T., & Gupta, V. K. (2012). Column with CNT/magnesium oxide composite for lead (II) removal from water. *Environmental Science and Pollution Research, 19*(4), 1224–1228.

Shirsath, S. R., Hage, A. P., Zhou, M., Sonawane, S. H., & Ashokkumar, M. (2011). Ultrasound assisted preparation of nanoclay bentonite-FeCo nanocomposite hybrid hydrogel: a potential responsive sorbent for removal of organic pollutant from water. *Desalination, 281*, 429–437.

Tavakoli, O., & Yoshida, H. (2005). Effective recovery of harmful metal ions from squid wastes using subcritical and supercritical water treatments. *Environmental Science & Technology, 39*(7), 2357–2363.

Uğuzdoğan, E., Baki Denkbaş, E., & Sermet Kabasakal, O. (2010). The use of polyethyleneglycolmethacrylate-co-vinylimidazole (PEGMA-co-VI) microspheres for the removal of nickel(II) and chromium(VI) Ions. *Journal of Hazardous Materials, 177*(1–3), 119–125.

Wang, L., Zhang, J., & Wang, A. (2008). Removal of methylene blue from aqueous solution using chitosan-*g*-poly(acrylic acid)/ montmorillonite superadsorbent nanocomposite. *Colloids and Surfaces A: Physicochemical and Engineering Aspects, 322*(1–3), 47–53.

Wang, X., Zheng, Y., & Wang, A. (2009). Fast removal of copper ions from aqueous solution by chitosan-*g*-poly(acrylic acid)/ attapulgite composites. *Journal of Hazardous Materials, 168*(2–3), 970–977.

Wu, N., Wei, H., & Zhang, L. (2012). Efficient removal of heavy metal ions with biopolymer template synthesized mesoporous titania beads of hundreds of micrometers size. *Environmental Science & Technology, 46*(1), 419–425.

Xu, K., Tan, Y., Chen, Q., An, H., Li, W., Dong, L., & Wang, P. (2010). A novel multi-responsive polyampholyte composite hydrogel with excellent mechanical strength and rapid shrinking rate. *Journal of Colloid and Interface Science, 345*(2), 360–368.

Xu, Z., Ren, T., Xiao, C., Li, H., & Wu, T. (2011). Nickel promotes the invasive potential of human lung cancer cells via TLR4/ MyD88 signaling. *Toxicology, 285*(1–2), 25–30.

Yan, H., Yang, L., Yang, Z., Yang, H., Li, A., & Cheng, R. (2012). Preparation of chitosan/poly(acrylic acid) magnetic composite microspheres and applications in the removal of copper(II) ions from aqueous solutions. *Journal of Hazardous Materials, 229–230*, 371–380.

Yoshizaki, S., & Tomida, T. (2000). Principle and process of heavy metal removal from sewage sludge. *Environmental Science & Technology, 34*(8), 1572–1575.

Zendehdel, M., Barati, A., & Alikhani, H. (2011). Removal of heavy metals from aqueous solution by poly(acrylamide-co-acrylic acid) modified with porous materials. *Polymer Bulletin, 67*(2), 343–360.

Zhang, C., Zhang, H., Wang, L., Zhang, J., & Yao, H. (2007a). Purification of antifreeze protein from wheat bran (*Triticum aestivum* L.) based on its hydrophilicity and ice-binding capacity. *Journal of Agricultural and Food Chemistry, 55*(19), 7654–7658.

Zhang, J., Wang, Q., & Wang, A. (2007b). Synthesis and characterization of chitosan-*g*-poly(acrylic acid)/attapulgite superabsorbent composites. *Carbohydrate Polymers, 68*(2), 367–374.

Zhang, D., Wang, D., Duan, J., & Ge, S. (2009). Research on the long time swelling properties of poly (vinyl alcohol)/hydroxyapatite composite hydrogel. *Journal of Bionic Engineering, 6*(1), 22–28.

Zhao, X., Jia, Q., Song, N., Zhou, W., & Li, Y. (2010). Adsorption of Pb(II) from an aqueous solution by titanium dioxide/ carbon nanotube nanocomposites: kinetics, thermodynamics, and isotherms. *Journal of Chemical & Engineering Data, 55*(10), 4428–4433.